280319b

Extrinsic Conditions Influence the Self-Association and Structure of IF_1, the Regulatory Protein of Mitochondrial ATP Synthase

Vytaute Boreikaite [a,b,1], Basile I. M. Wicky [b,1], Ian N. Watt [a], Jane Clarke[b] and John E. Walker [a,2]

[a]*The Medical Research Council Mitochondrial Biology Unit, University of Cambridge, Cambridge Biomedical Campus, Hills Road, Cambridge CB2 0XY, United Kingdom;*

[b]*The Department of Chemistry, University of Cambridge, Lensfield Road, Cambridge CB2 1EW, United Kingdom*

[1]Equal contributions

[2]To whom correspondence should be addressed. J. E. W., Tel.: +44-1223-252701; e-mail: walker@mrc-mbu.cam.ac.uk

Running title: Inhibitor protein of ATP synthase

The authors declare no conflict of interest

Author contributions: J. E. W. and B. I. M. W. designed research; J. E. W., B. I. M. W. and J. C. supervised project; V. B., I. N. W. and B. I. M. W. performed research; V. B. and B. I. M. W. analyzed data; V. B. and B. I. M. W. and J. E. W. wrote the text.

Key words: Mitochondria; ATP hydrolysis; regulation; inhibitor; intrinsically disordered protein

Significance statement

Adenosine triphosphate (ATP), the fuel of biology, is produced by a molecular machine with a rotary action. Inside the mitochondria of eukaryotic cells, rotation is driven by a proton motive force across the inner membranes of the organelle generated by oxidation of sugars and fats in food. Under anoxic conditions, the rotary machine hydrolyzes ATP and reverses rotation. This wastage is prevented by an intrinsically disordered region of the inhibitor protein, IF_1, which inserts itself in the machine and stops reverse rotation. The inhibitory activity of IF_1 is regulated by self-association, which is influenced by pH and ion-types, providing a potential molecular mechanism for the modulation of ATPase activity by cellular physiology via this solution-responsive, self-associating protein. [117 words]

Summary

The endogenous inhibitor of ATP synthase in mitochondria, known as IF_1, conserves cellular energy when the proton motive force collapses by inhibiting ATP hydrolysis. Around neutrality, the 84 amino acid bovine IF_1 is thought to self-assemble into active dimers, and under alkaline conditions into inactive tetramers and higher oligomers. Dimerization is mediated by formation of an anti-parallel α-helical coiled-coil involving residues 44-84. The inhibitory region of each monomer from residues 1-46 is largely α-helical in crystals, but disordered in solution. The formation of the inhibited enzyme complex requires the hydrolysis of two ATP molecules, and in the complex the disordered region from residues 8-13 is extended and is followed by an α-helix from residues 14-18, and a longer α-helix from residue 21, which continues unbroken into the coiled-coil region. From residues 21-46, the long α-helix binds to other α-helices in C-terminal region of predominantly one of the β-subunits in the most closed of the three catalytic interfaces. The definition of the factors that influence the self-association of

IF_1 is a key to understanding the regulation of its inhibitory properties. Therefore, we investigated the influence of pH and salt-types on the self-association of bovine IF_1 and the folding of its unfolded region. We identified the equilibrium between dimers and tetramers as a potential central factor in the *in vivo* modulation of the inhibitory activity, and suggest that the intrinsically disordered region makes its inhibitory potency exquisitely sensitive and responsive to physiological changes that influence the capability of mitochondria to make ATP. [250 words]

Introduction

The mitochondrial ATP synthases, also known as F-ATPases or F_1F_o-ATPases, are multi-subunit enzymes found in the inner membranes of the organelle (1, 2). Under aerobic conditions, they make ATP from ADP and phosphate using a proton-motive force (pmf) generated by respiration, as a source of energy to drive their rotary mechanism. If the pmf is dissipated, for example during ischemia, the enzyme reverses its direction of rotation, and starts to hydrolyze ATP, but this hydrolytic activity becomes inhibited by a protein known as IF_1 (3). The active state, which is present at pH values around neutrality (4), binds to one of the three catalytic sites of the membrane extrinsic F_1-domain of the enzyme, stopping hydrolysis (5, 6). Bovine IF_1 is a basic protein of 84 amino acids (7, 8). In a structure of bovine F_1-ATPase inhibited with a monomeric fragment consisting of residues 1-60 of bovine IF_1, residues 1-46 are bound in one of the three catalytic interfaces of the enzyme with the N-terminal region of the inhibitor penetrating from outside the enzyme into an internal aqueous cavity surrounding part of the enzyme's rotor (6). Residues 1-7 of IF_1 were unresolved, residues 8-13 form an extended structure, linked to an α-helix from residues 14-18 that interacts with the γ-subunit in the rotor. This α-helix is attached by a turn from residues 19-20 to a second α-helix from residues 21-50, which interacts with other α-helices in

the C-terminal domains of the α- and β-subunits in the $\alpha_{DP}\beta_{DP}$-catalytic interface, the most closed of the three catalytic interfaces. From residues 47-50, the long α-helix extends beyond the surface of the enzyme, and the remainder of truncated IF_1 was unresolved. In crystals of IF_1 alone, the protein is disordered from residues 1-18 and α-helical from residues 19-83, and is dimerized by an anti-parallel α-helical coiled-coil from residues 44-84 (9). The dimers form tetramers and higher oligomers, and the formation of tetramers occludes the N-terminal inhibitory region. In solution, the dimerization of dimers and occlusion of the inhibitory region is pH dependent (4). At pH values below about 7.5, IF_1 is an active dimer, and at higher pH values tetramers and oligomers form, and IF_1 is inactive. The mutation H49K (10) abolishes the ability to form tetramers and the mutated dimeric IF_1 is constitutively active and pH independent (4). In solution, the C-terminal region of IF_1 forms a dimeric α-helical coiled-coil on its own, whereas the N-terminal inhibitory region is unstructured (11), and provides an example of an intrinsically disordered protein (IDP) (12). During inhibition of F_1-ATPase, the disordered region interacts with the most open of the three catalytic sites and becomes α-helical from residues 31-49. Hydrolysis of two ATP molecules converts this open site with bound IF_1, to first, a partially closed site, where residues 23-50 of IF_1 are α-helical region, and then to the fully closed state, where the inhibitory region is structured to its greatest extent (12).

IDPs are characterized by a lack of defined structure, and they populate many different conformational states (13, 14). They are prevalent, especially in higher eukaryotes, and they are functional, and more responsive to solution conditions than folded proteins. Factors such as ionic strength (15), pH (16), temperature (17), and molecular crowding (18) all have an impact on IDPs by influencing, for example, their radius of gyration and the collapse of unfolded polypeptide chains. These enhanced

sensitivities to environmental factors can be ascribed to their shallower energy landscapes, and these factors can influence directly the binding profiles of coupled folding and binding processes (19), as with the influence of pH on the oligomeric state of IF_1 (4). Mitochondria respond to changes in physiological conditions by taking up and releasing Ca^{2+}, K^+ and other cations via specific channels (20). Therefore, as described here, we have studied the influence of pH and cationic-types on the structure and oligomeric state of IF_1 in solution.

Results

Dependence of the Oligomerization of IF_1 on pH. The oligomeric state of IF_1 was investigated by covalent cross-linking IF_1-Y33W and IF_1-Y33W-H49K with 1-ethyl-3-(3-dimethylaminopropyl)-carbodiimide (EDC) from pH 3.3-8.0. The mutation Y33W has no effect on the inhibitory properties of the protein (21). Around neutral pH, IF_1-Y33W formed tetramers, whereas IF_1-Y33W-H49K was primarily dimeric (*SI Appendix*, Fig. S1*A*). With decreasing pH, IF_1-Y33W dissociated to dimers and ultimately both proteins became monomeric. As the multimeric species were most abundant at neutral pH, which is beyond the optimal range for the reactivity of EDC from pH 4.6 to 6.0, these results report on the effect of pH on the oligomerization of IF_1, and not on the chemical reactivity of the cross-linker.

Covalent cross-linking provides information about the presence or absence of given species, but does not reflect the distribution of oligomeric states in solution at equilibrium. Therefore, analytical ultracentrifugation (AUC) was performed at pH 2.4, 4.0, and 6.9 (*SI Appendix*, Fig. S1*B,* Fig. S2, Table S1). At pH 2.4, both IF_1-Y33W and IF_1-Y33W-H49K were monomeric. At pH 4.0, both proteins had similar sedimentation coefficients, and their estimated masses were consistent with coalesced distributions of monomeric and dimeric species. At pH 6.9, the behaviour of the two proteins diverged

markedly with IF_1-Y33W having a much larger sedimentation coefficient than at pH 4.0, consistent with it being tetrameric, whereas the value for IF_1-Y33W-H49K did not change extensively, and indicated that it was dimeric. The fractional ratio (f/f_0) of both proteins diminished with increasing pH values, indicative of the formation of more folded structures. Thus, this work confirmed that the oligomeric state of IF_1 is dependent on pH, and the mutation H49K suppresses tetramerization.

Effect of pH on the Structure of IF_1. Circular dichroism (CD) spectroscopy allows the bulk secondary structure profiles of proteins to be determined, and is particularly sensitive to the α-helical content. Both IF_1-Y33W and IF_1-Y33W-H49K underwent a helix-coil transition as a function of pH (Fig. 1 *A* and *B*). At pH 2.0, the spectra of both proteins were consistent with the presence of unfolded states containing some residual helicity (~18%). In contrast, towards neutral pH about 70% of the proteins were α-helical. The degree of helicity of IF_1-Y33W-H49K and IF_1-Y33W did not differ greatly, suggesting that the tetramer is not folded much more than the dimer. No changes in structure were observed in the alkaline region up to about pH 10 (*SI Appendix*, Fig. S3).

Dependence of the pH-Induced Coil-to-Helix Transition on Protein Concentration. To confirm that the loss of secondary structure observed by CD was related to the disassembly of the oligomers detected by AUC and cross-linking, pH profiles of IF_1-Y33W and IF_1-Y33W-H49K were measured at protein concentrations spanning two orders of magnitude (1-100 μM). A clear shift of the transition midpoint (Fig. 1 *C* and *D*) is consistent with concentration-dependent events. The pH profiles of both IF_1-Y33W and IF_1-Y33W-H49K have single transitions, consistent with concomitant folding and oligomerization. The single transition with IF_1-Y33W also suggests that the formation of dimers and tetramers as a function of pH is either

cooperative, or that the events are merged significantly. Thus, it appears that the stabilities of the dimeric and tetrameric species are similar with respect to pH.

To confirm the results from CD spectroscopy, IF_1-Y33W and IF_1-Y33W-H49K were reacted with EDC at the same 100-fold range of protein concentrations and at pH values of 5.3 and 7.0. As expected, oligomers were more abundant at higher protein concentrations, confirming the concentration-dependence of the oligomerization of IF_1 observed by CD (*SI Appendix*, Fig. S4).

Role of the C-terminal Region of IF_1 in Oligomerization. The role of the C-terminal part of IF_1 and the effect of pH on the formation of oligomers of IF_1 was studied with I1-62-Y33W-H49K and I1-62-Y33W, versions of IF_1 that are C-terminally truncated at residue 62 and lack the capacity to dimerize, with and without the mutation H49K. The pH profiles and concentration dependence of both proteins revealed disordered structures under all conditions of pH and protein concentrations investigated (*SI Appendix*, Fig. S5 *A* and *B*). Importantly, the residual helicity was almost entirely independent of either parameter (*SI Appendix*, Fig. S5*C*). These results are consistent with unfolded monomers, as confirmed by covalent cross-linking, which revealed virtually no oligomeric species (*SI Appendix*, Fig. S5*D*). Thus, the C-terminal region is required for both dimerization and tetramerization of IF_1.

Energetics of Oligomerization of IF_1. The oligomerization of IF_1 was studied quantitatively by chemical denaturation with urea. Chemical denaturation has been used extensively to study the folding stability of both monomeric proteins and oligomers (22–24). However, beyond dimers, the mathematical formulation for data analysis becomes less trivial, and fewer systems have been investigated (25, 26). Here, models describing two-state (monomer/dimer) homo-dimerization, two-state (monomer/tetramer) homo-tetramerization and three-state (monomer/dimer/tetramer)

homo-tetramerization were developed (see *SI Appendix*, Supplementary Methods), allowing equilibrium constants between the different oligomeric states to be obtained from the chemical denaturation data. Denaturation with urea of IF_1-Y33W and IF_1-Y33W-H49K produced single transitions, and their positions depended on the protein concentration, as expected for oligomeric species (Fig. 2 *A* and *B*). Cross-linking experiments in the presence of urea confirmed that the spectral changes observed by CD were associated with the dissociation of oligomers of IF_1 (*SI Appendix*, Fig. S6). The reversibility of chemical denaturation was confirmed in a refolding experiment (*SI Appendix*, Fig. S7).

The CD spectral signatures of each species (the baselines) in denaturation experiments hold structural information. Thus, the α-helical contents estimated from molar residue ellipticity (MRE) values at 222 nm revealed that at pH 7.0, the tetramer and dimer were ~72% and ~62% α-helical, respectively (folded species), whereas the monomers were ~12% α-helical (consistent with a disordered protein). Thus, the oligomerization of IF_1 is a coupled folding and binding reaction where monomers cannot fold autonomously, and acquire their α-helical structures by self-assembly. Even at neutral pH, the monomeric state of the protein is unfolded, confirming that IF_1 on its own is an IDP.

Effect of pH on Tetramerization and Dimerization. Equilibrium denaturation curves of IF_1-Y33W and IF_1-Y33W H49K at pH values of 6.0, 7.0 and 8.0 were obtained, and the data for IF_1-Y33W-H49K were fitted to the two-state homo-dimerization model (Fig. 2 *C* and *D*), and the extracted free energies of oligomerization extracted were converted to K_d values (Fig. 3*A;* Tables 1 and S2). The affinity of the dimer of IF_1-Y33W-H49K was in the low nanomolar regime. More acidic conditions destabilized

the dimer, as expected from the qualitative results. However, over the pH range of 6-8, the K_d value was relatively insensitive to pH, changing only by 4-fold.

The spectroscopic signatures for the dimer and the tetramer species are similar (*vide supra*), and there was no clear biphasic transition for the chemical denaturation of IF_1-Y33W. Thus, it was not obvious whether or not a dimeric intermediate is populated at equilibrium. However, the chemical denaturation data of IF_1-Y33W were best described by the three-state tetramerization model (*SI Appendix*, Supplementary Methods) (Fig. 2*C*; Tables S3-S5). Since this model explicitly describes a dimeric intermediate, the effects of pH on the tetramerization (tetramer to dimer) and on the dimerization (dimer to monomer) of IF_1-Y33W could be quantified (Table 2). As with IF_1-Y33W-H49K, dimerization was relatively insensitive to pH, and the affinity only varied by ~5-fold over the pH range investigated. In contrast, the affinity of the tetrameric species varied by three orders of magnitude over the same pH range, demonstrating that it is the extent of tetramerization, and not dimerization, that is modulated primarily by pH.

As the K_d values for the tetramer formation and for the dimer formation of IF_1-Y33W are close in magnitude, the dimeric intermediate is never populated on its own under the conditions investigated, consistent with the lack of a biphasic transition in the unfolding data. Nevertheless, the differential effect of pH on the affinities of the tetramer and dimer species signifies that the fraction of the dimer present varies greatly as a function of pH (Fig. 3*B*). Thus, even a relatively small change in solution conditions can have a dramatic impact on the distribution of oligomeric states, which in turn is likely to affect the extent of inhibition of the hydrolytic activity of the ATP synthase by IF_1.

Cation Dependence of the Stability of Oligomers. Samples of IF_1-Y33W and IF_1-Y33W-H49K were melted in the presence of various salts at a constant ionic strength of 1 M and neutral pH, and the disassembly of IF_1 oligomers was followed as a loss of helicity by CD spectroscopy at 222 nm (Fig. 4 *A* and *B*). Disassembly was influenced by cations, and the order of stability followed the Hofmeister series, calcium ions having the strongest destabilizing effect, as observed with other IDP systems (19). Moreover, the shift in the midpoint of the unfolding transition was more pronounced for IF_1-Y33W than for IF_1-Y33W-H49K, suggesting that the tetramer is more sensitive than the dimer to ionic conditions. This observation echoes the results obtained for pH sensitivity of the different oligomeric transitions.

To gain a quantitative understanding of the effects of ion-types, dissociation constants were estimated from chemical denaturation experiments. Sodium ions and calcium ions were investigated at two values of ionic strength, as was the absence of any salt (Fig. 4*C*). In all cases, calcium ions had a stronger destabilizing effect than sodium, consistent with the Hofmeister series and the thermal melt experiments. As expected from the Hofmeister effect, higher ionic strengths led to greater differences between sodium and calcium. Thus, the oligomerization of IF_1 is influenced by the nature of the surrounding cations.

Discussion

Qualitatively the oligomerization of IF_1 depends upon pH. At neutrality, the pseudo-wild-type inhibitor protein, IF_1-Y33W was tetrameric, and the mutant inhibitor IF_1-Y33W-H49K was dimeric. These oligomers disassembled with decreasing pH. However, minor deviations of pH towards acidic values had important effects on the assemblage of oligomeric states. In contrast, changes of pH of the same magnitude towards increasingly alkaline values had very little effect, highlighting the sensitivity

of the state of IF_1 to acidic environments. These effects probably relate to the biological function of IF_1, as its oligomeric states inhibit the hydrolytic activity of ATP synthase to different extents (4).

However, the oligomerization of IF_1 is not simply the association of folded monomers, and the folding and self-association processes are coupled. Under conditions where the protein was monomeric, it was also disordered. Therefore, the protein cannot fold autonomously, and it gains helicity by forming inter-chain contacts. Thus, we emphasize that the thermodynamic parameters relating to the dimer/monomer transition reported here contain the contributions from both folding and binding, and that these cannot be deconvoluted. The obligate multimeric nature of the folding event also implies that the stability of the structured state(s) is (are) concentration-dependent, as confirmed by the transition mid-point of the pH curve being a function of the total protein concentration. As the extents of helicity of the dimer and tetramer appear to be similar, this additional oligomerization step appears not to contribute significantly to folding.

The multimeric nature of IF_1 has important implications for the stability of its structured state(s), and protein concentration will influence the distribution of oligomeric species at equilibrium, probably affecting the inhibitory potency of IF_1. Thus, oligomerization was quantified as a function of pH by chemical denaturation. This approach for studying IF_1 was validated, and quantitative models were developed for both dimerization and tetramerization. The pseudo-wild-type IF_1-Y33W gave a single transition, suggesting a fully cooperative transition of tetramer to monomer. However, the two-state model did not properly capture the data, suggesting the presence of a lowly-populated intermediate (a complete discussion of the shortcomings of the two-state tetramerization model can be found in Supplementary Methods). Given all

the other independent supporting evidence, this intermediate was assigned as the dimer, and the data fitted to a three-state tetramerization model.

Quantitatively, the influence of pH on the assembly of both IF_1-Y33W and IF_1-Y33W H49K differed markedly. Whereas the dimerization of both proteins was relatively insensitive in the pH range 6-8 (with K_d values varying by only 4-5-fold), the tetramerization of IF_1-Y33W was extremely sensitive (the K_d value varied about 1700-fold over the same pH range). Therefore, it is the extent of tetramerization, and not dimerization, that is affected most strongly by changes in pH within the physiological range. All five histidine residues of IF_1 are in its C-terminal region, and, in the structure of IF_1, this region is involved in dimerization via an antiparallel α-helical coil-coil. In bovine $IF_1$1-60, the pK_a values of these histidines are in the range of 6.2-6.8 (11). Thus, changes in pH might be expected to affect dimerization strongly, with increasing protonation of these residues affecting primarily the stability of the dimer. However, it is the tetramer/dimer transition that is most affected in solution. The greater number of protein chains present in the tetramer, and the resulting additive effect of protonating a histidine site per chain could explain this behaviour. Moreover, if these histidines were in close spatial proximity in the structure of the tetramer, these effects would become non-additive, and could compound in terms of stability, resulting in even greater sensitivity. However, for this to be the case, the structure of the IF_1 tetramer in solution would have to be different from the fibrillar crystal structure where such contacts are absent (9).

At the values of pH investigated here, the magnitudes of the K_d values for the tetramer and dimer species of IF_1-Y33W are relatively similar, and therefore the dimeric intermediate is never present on its own, representing a fraction of the total protein concentration. However, because of the differential effect of pH on the affinities

of the tetramerization and dimerization events, the fraction of dimer varies greatly with pH (Fig. *4B*). At a concentration of a 100 nM, for example, the distribution at pH 8.0 is ~80 % tetramer and ~10 % for both monomer and dimer. At pH 6.0, this distribution has changed to <5 % tetramer, and ~50 % of both monomer and dimer. However, not all protein concentrations give rise to similar redistributions. For example, at a protein concentration of IF_1 of 10 nM, the fraction of dimer never exceeds ~20 %, regardless of pH. Thus, the population of oligomeric states in the mitochondrial matrix at a particular pH value will depend on the total concentration of IF_1 in the organelle. Whilst these observations are likely to be physiologically relevant, as yet, there are no accurate estimates of the *in organello* concentrations of IF_1, although it is clearly an abundant protein (27).

Another potentially physiologically relevant finding is that the oligomeric stability of IF_1 is sensitive to both ionic strength and the nature of surrounding cationic species. As in other IDP systems (19), the order of stability followed the Hofmeister series. Most significantly, the presence of mM concentrations of Ca^{2+} had a significant destabilizing effect, especially on tetramerization. Although the changes were relatively modest (a few fold), and the observations were made at pH 7.0, it seems probable that at more acidic pH values, where the stability of the oligomers is already marginal, the effects of cations will become more pronounced. Thus, in mitochondria, it is likely that the oligomeric state of IF_1 and its inhibitory potency are modulated by a combination of pH and cation-type. Moreover, the intrinsically disordered nature of the inhibitory region of IF_1 makes that inhibitory potency exquisitely sensitive and responsive to any physiological changes that may influence the capability of the mitochondria to make ATP. The concentrations of free cations in the mitochondrial matrix are difficult to estimate because of the presence of phosphate at changing levels, and also of proteins,

DNA and RNA molecules. Nonetheless, it is generally assumed that the concentration of K^+ ions is about 100 mM, similar to the cytosol (28). One estimate of the concentration of free Mg^{2+} in the mitochondrial matrix is that it is about 0.67 mM (29) and that of Na^+ about 10 mM (30). The concentration of cytoplasmic Ca^{2+} in most cells is 0.05-0.5 μM, and the mitochondria act as a temporary store for Ca^{2+} in the form of a calcium phosphate gel when the mitochondrial concentration exceeds a set point, which varies from 0.3-1 μM (28). In the mitochondrial concentration range of 0.1-1 μM, Ca^{2+} regulates the activities of three central mitochondrial enzymes, pyruvate dehydrogenase, isocitrate synthase and 2-oxoglutarate dehydrogenase (31). It now seems likely that the influx of Ca^{2+} into mitochondria has a fourth important physiological role in increasing the inhibitory potency of IF_1, leading to the rapid inactivation of the ATPase, as observed earlier (32).

Materials and Methods

Variants of bovine IF_1 were expressed and purified as described previously (4), and characterized by mass spectrometry (*SI Appendix*, Table *S6*). The oligomeric state of proteins was examined by covalent cross-linking and analytical centrifugation. The helicity of proteins was determined by CD spectroscopy**.** Proteins were denatured with urea and CD spectra were recorded at intervals. Changes in MRE_{222} as a function of urea concentration were fitted to appropriate homo-oligomerization models to extract thermodynamic parameters by non-linear least squares minimization routines (*SI Appendix*, Tables S2-S4). For further details, see *SI Appendix*.

ADDITIONAL INFORMATION

The authors declare no conflict of interest.

Acknowledgements

We thank Dr. K. Stott and Mr. P. Sharratt (both Department of Chemistry, University of Cambridge) for assistance with the AUC experiments and amino acid analysis, respectively; and Dr. S. Ding and Mr M. G. Montgomery (both MRC Mitochondrial Biology Unit, Cambridge) for measuring molecular masses and help in preparing the manuscript, respectively. B. I. M. W. was supported by the Cambridge Trust, St Catharine's College, Cambridge and the Cambridge Philosophical Society. J. C. is a Wellcome Trust Senior Fellow. This work was supported by the Medical Research Council, U. K. by grants MC_U105663150 and MR/M009858/1 to J. E. W. and by the Wellcome Trust by grant WT095195 to J. C.

REFERENCES

1. Walker JE (2013) The ATP synthase: the understood, the uncertain and the unknown. *Biochem Soc Trans* 41(1):1–16.
2. Walker JE (2017) Structure, Mechanism and Regulation of ATP synthases. *Mechanisms of Primary Energy Transduction in Biology*, ed Wikström M (Royal Society of Chemistry, Cambridge), pp 338–373.
3. Pullman ME, Monroy GC (1963) A naturally occuring inhibitor of mitochondrial adenosine triphosphate. *J Biol Chem* 238:3762–3769.
4. Cabezon E, Butler PJ, Runswick MJ, Walker JE (2000) Modulation of the oligomerization state of the bovine F_1-ATPase inhibitor protein, IF_1, by pH. *J Biol Chem* 275(33):25460–25464.

5. Cabezón E, Montgomery MG, Leslie AGW, Walker JE (2003) The structure of bovine F_1-ATPase in complex with its regulatory protein IF_1. *Nat Struct Biol* 10(9):744–750.

6. Gledhill JR, Montgomery MG, Leslie AGW, Walker JE (2007) How the regulatory protein, IF_1, inhibits F_1-ATPase from bovine mitochondria. *Proc Natl Acad Sci U S A* 104(40):15671–15676.

7. Frangione B, Rosenwasser E, Penefsky HS, Pullman ME (1981) Amino acid sequence of the protein inhibitor of mitochondrial adenosine triphosphatase. *Proc Natl Acad Sci U S A* 78(12):7403–7407.

8. Walker JE, Gay NJ, Powell SJ, Kostina M, Dyer MR (1987) ATP synthase from bovine mitochondria: sequences of imported precursors of oligomycin sensitivity conferral protein, factor 6, and adenosinetriphosphatase inhibitor protein. *Biochemistry* 26:8613–8619.

9. Cabezón E, Runswick MJ, Leslie AGW, Walker JE (2001) The structure of bovine IF_1, the regulatory subunit of mitochondrial F-ATPase. *EMBO J* 20(24):6990–6996.

10. Schnizer R, Van Heeke G, Amaturo D, Schuster SM (1996) Histidine-49 is necessary for the pH-dependent transition between active and inactive states of the bovine F_1-ATPase inhibitor protein. *Biochim Biophys Acta* 1292(2):241–248.

11. Gordon-Smith DJ *et al.* (2001) Solution structure of a C-terminal coiled-coil domain from bovine IF_1: the inhibitor protein of F_1 ATPase. *J Mol Biol* 308(2):325–339.

12. Bason JV, Montgomery MG, Leslie AGW, Walker JE (2014) Pathway of binding of the intrinsically disordered mitochondrial inhibitor protein to F_1-ATPase. *Proc Natl Acad Sci U S A* 111(31):11305–11310.

13. Eliezer D (2009) Biophysical characterization of intrinsically disordered proteins. *Curr Opin Struct Biol* 19(1):23–30.

14. van der Lee R *et al.* (2014) Classification of intrinsically disordered regions and proteins. *Chem Rev* 114(13):6589–6631.

15. Müller-Späth S *et al.* (2010) From the Cover: Charge interactions can dominate the dimensions of intrinsically disordered proteins. *Proc Natl Acad Sci U S A* 107(33):14609–14614.

16. Hofmann H, Nettels D, Schuler B (2013) Single-molecule spectroscopy of the unexpected collapse of an unfolded protein at low pH. *J Chem Phys* 139(12):121930.

17. Wuttke R *et al.* (2014) Temperature-dependent solvation modulates the dimensions of disordered proteins. *Proc Natl Acad Sci U S A* 111(14):5213–5218.

18. Soranno A *et al.* (2014) Single-molecule spectroscopy reveals polymer effects of disordered proteins in crowded environments. *Proc Natl Acad Sci U S A* 111(13):4874–4879.

19. Wicky BIM, Shammas SL, Clarke J (2017) Affinity of IDPs to their targets is modulated by ion-specific changes in kinetics and residual structure. *Proc Natl Acad Sci U S A* 114(37):9882–9887.

20. Szabo I, Zoratti M (2014) Mitochondrial channels: ion fluxes and more. *Physiol Rev* 94(2):519–608.

21. Bason JV, Runswick MJ, Fearnley IM, Walker JE (2011) Binding of the inhibitor protein IF_1 to bovine F_1-ATPase. *J Mol Biol* 406(3):443–453.

22. Gardner NW, Monroe LK, Kihara D, Park C (2016) Energetic Coupling between Ligand Binding and Dimerization in Escherichia coli Phosphoglycerate Mutase. *Biochemistry* 55(12):1711–1723.

23. Gloss LM, Matthews CR (1997) Urea and thermal equilibrium denaturation studies on the dimerization domain of Escherichia coli Trp repressor. *Biochemistry* 36(19):5612–5623.

24. Mallam AL, Jackson SE (2005) Folding studies on a knotted protein. *J Mol Biol* 346(5):1409–1421.

25. Guidry JJ, Moczygemba CK, Steede NK, Landry SJ, Wittung-Stafshede P (2000) Reversible denaturation of oligomeric human chaperonin 10: denatured state depends on chemical denaturant. *Protein Sci* 9(11):2109–2117.

26. Simler BR, Doyle BL, Matthews CR (2004) Zinc binding drives the folding and association of the homo-trimeric gamma-carbonic anhydrase from Methanosarcina thermophila. *Protein Eng Des Sel* 17(3):285–291.

27. Rouslin W, Frank GD, Broge CW (1995) Content and binding characteristics of the mitochondrial ATPase inhibitor, IF_1, in the tissues of several slow and fast heart-rate homeothermic species and in two poikilotherms. *J Bioenerg Biomembr* 27(1):117–125.

28. Nicholls DG, Ferguson SJ (2013) *Bioenergetics 4* (Academic Press, Cambridge, Massachusetts, USA).

29. Jung DW, Panzeter E, Baysal K, Brierley GP (1997) On the relationship between matrix free Mg^{2+} concentration and total Mg^{2+} in heart mitochondria. *Biochim Biophys Acta* 1320(3):310–320.

30. Donoso P, Mill JG, O'Neill SC, Eisner DA (1992) Fluorescence measurements of cytoplasmic and mitochondrial sodium concentration in rat ventricular myocytes. *J Physiol* 448:493–509.

31. Denton RM, McCormack JG (1980) On the role of the calcium transport cycle in heart and other mammalian mitochondria. *FEBS Lett* 119(1):1–8.

32. De Gómez-Puyou MT, Gavilanes M, Gómez-Puyou A, Ernster L (1980) Control of activity states of heart mitochondrial ATPase. Role of the proton-motive force and Ca^{2+}. *Biochim Biophys Acta* 592(3):396–405.

33. Bernadó P, Blackledge M, Sancho J (2006) Sequence-specific solvent accessibilities of protein residues in unfolded protein ensembles. *Biophys J* 91(12):4536–4543.

34. Estrada J, Bernadó P, Blackledge M, Sancho J (2009) ProtSA: a web application for calculating sequence specific protein solvent accessibilities in the unfolded ensemble. *BMC Bioinformatics* 10:104.

35. Myers JK, Pace CN, Scholtz JM (1995) Denaturant m values and heat capacity changes: relation to changes in accessible surface areas of protein unfolding. *Protein Sci* 4(10):2138–2148.

36. Silvester JA, Dickson VK, Runswick MJ, Leslie AGW, Walker JE (2006) The expression, purification, crystallization and preliminary X-ray analysis of a subcomplex of the peripheral stalk of ATP synthase from bovine mitochondria. *Acta Cryst F* 62(Pt 6):530–533.

37. Pace CN (1986) Determination and analysis of urea and guanidine hydrochloride denaturation curves. *Methods Enzymol* 131:266–280.

38. Laue T, Shah B, Ridgeway T, Pelletier S (1992) Analytical ultracentrugation in biochemistry and polymer science. eds Harding SE, Rowe AJ, Horton JC (The Royal Society of Chemistry, Cambridge), pp 90–125.

39. Schuck P (2000) Size-distribution analysis of macromolecules by sedimentation velocity ultracentrifugation and lamm equation modeling. *Biophys J* 78(3):1606–1619.

40. Muñoz V, Serrano L (1995) Elucidating the folding problem of helical peptides using empirical parameters. III. Temperature and pH dependence. *J Mol Biol* 245(3):297–308.

41. Tanford C (1968) Protein denaturation. *Adv Protein Chem* 23:121–282.

42. Spudich G, Marqusee S (2000) A change in the apparent m value reveals a populated intermediate under equilibrium conditions in Escherichia coli ribonuclease HI. *Biochemistry* 39(38):11677–11683.

43. Soulages JL (1998) Chemical denaturation: potential impact of undetected intermediates in the free energy of unfolding and m-values obtained from a two-state assumption. *Biophys J* 75(1):484–492.

FIGURES

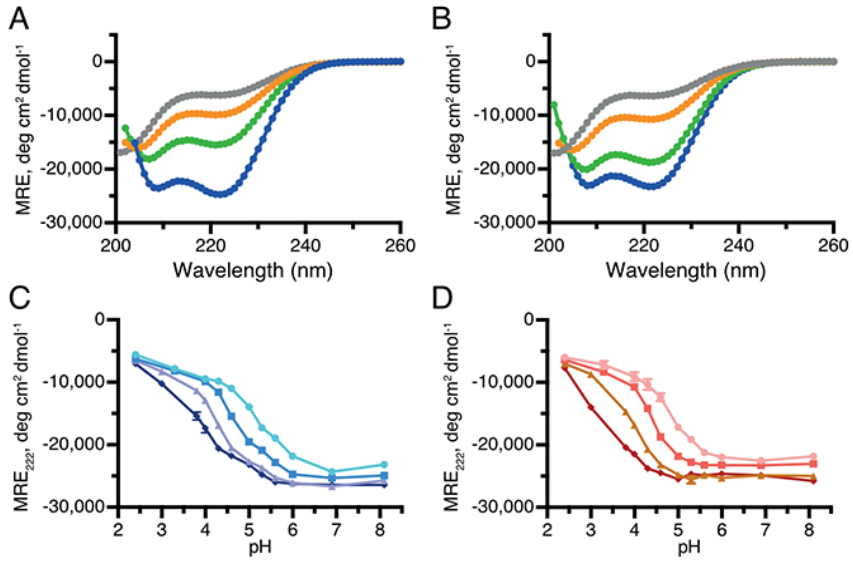

Fig. 2. Changes in secondary structure induced by pH. (*A*)-(*B*), CD spectra of IF_1-Y33W and IF_1-Y33W-H49K, respectively, at protein concentrations of 10 μM and pH values of 2.4 (grey), 4.0 (orange), 4.6, (green) and 6.0 (blue); (*C*)-(*D*), dependence of helicity of IF_1-Y33W and IF_1-Y33W-H49K, respectively, on pH at various protein concentrations. IF_1-Y33W: 1 μM; 10 μM; 50 μM; 100 μM. IF_1-Y33W-H49K: 1 μM; 10 μM; 50 μM; 100 μM. In (*C*) and (*D*), error bars denote the range of values measured.

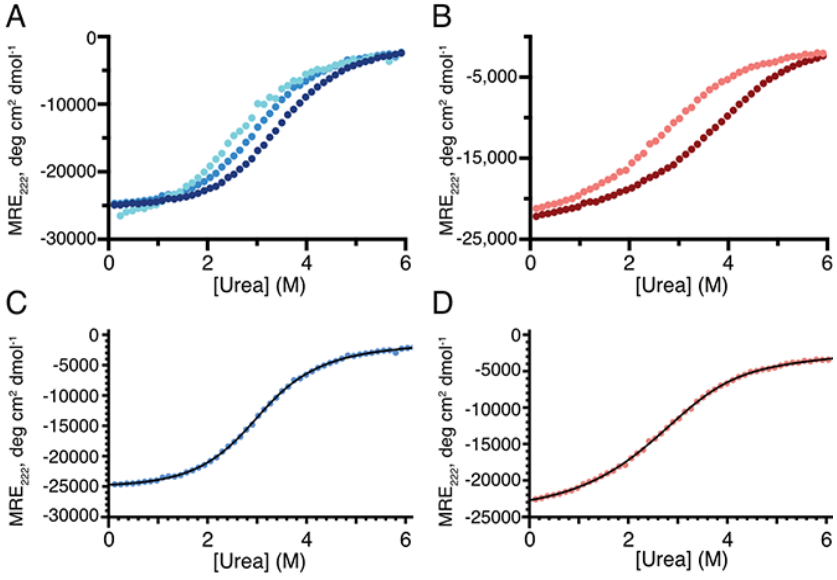

Fig. 3. Chemical denaturation of IF_1-Y33W and IF_1-Y33W-H49K. (*A*) and (*B*), urea denaturation at pH 7.0 of IF_1-Y33W and IF_1-Y33W-H49K, respectively, at various concentrations of proteins. (*A*) 1 μM (light blue), 3 μM (medium blue) and 9 μM (dark blue); (*B*), 1 μM (light red), 10 μM (dark red). (*C*)-(*D*), representative fittings of data from chemical denaturation at pH 7.0 of IF_1-Y33W (3 μM; blue) and IF_1-Y33W-H49K (1 μM; red), respectively. Fitted curves are depicted in black, and the colored dots are experimental values.

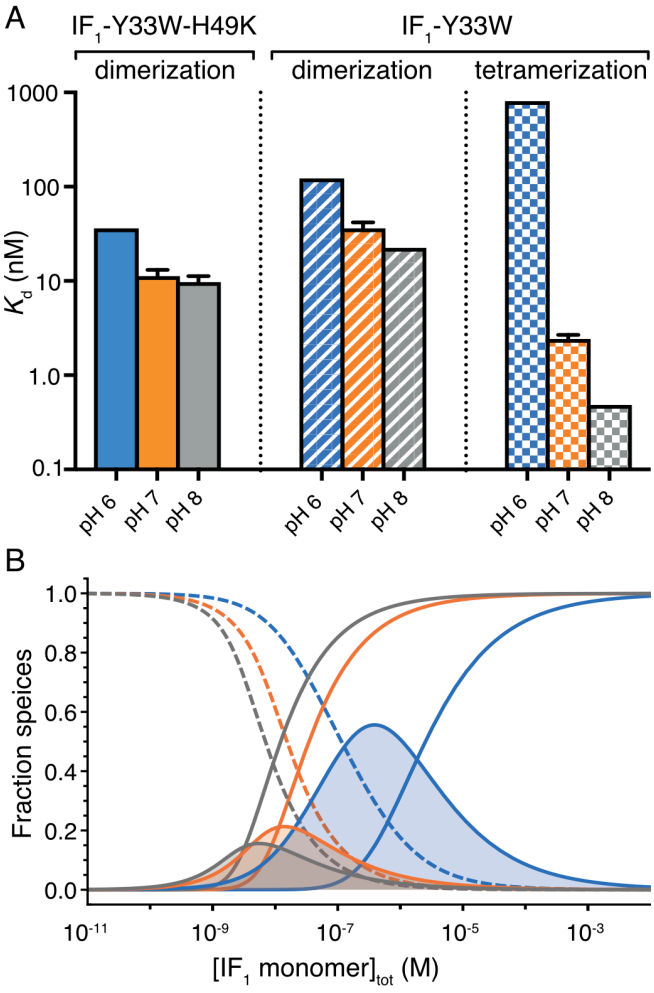

Fig. 4. Effect of pH on dimerization and tetramerization of IF_1. (*A*) Values of K_d for IF_1-Y33W and IF_1-Y33W-H49K at pH 6.0, 7.0, 8.0 obtained from chemical denaturation experiments. (*B*) Simulation of fractional oligomeric distribution for IF_1-Y33W at pH 6.0 (blue), pH 7.0 (orange) and pH 8.0 (grey). The monomeric, dimeric,

and tetrameric species are indicated as dashed, solid with filled areas beneath, and solid lines, respectively.

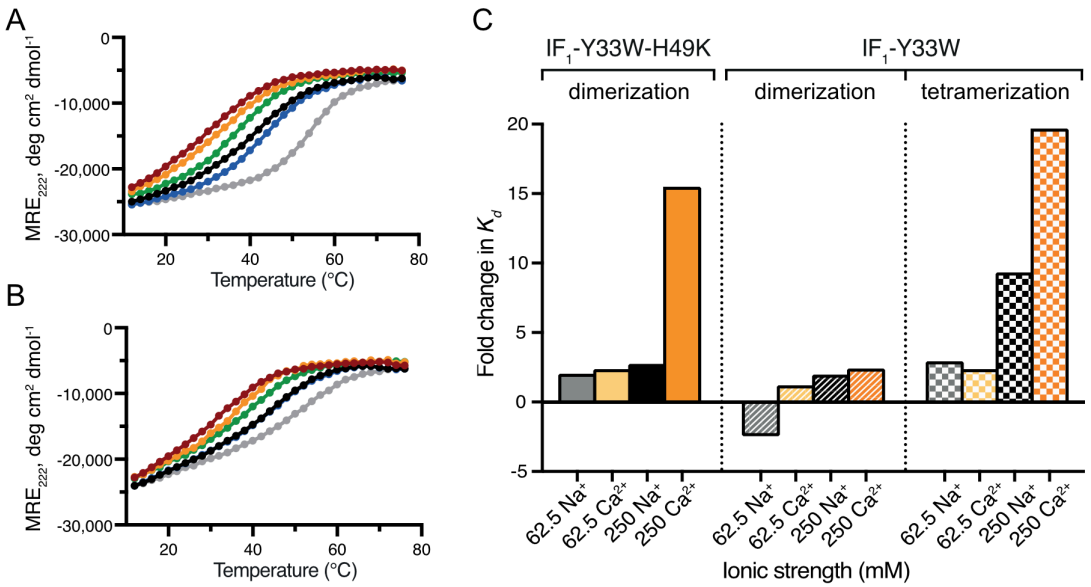

Fig. 5. Effect of ionic strength and cation-type on the oligomerization of IF_1. (*A*) and (*B*), thermal denaturation of IF_1-Y33W and IF_1-Y33W-H49K respectively. Unfolding was assessed by monitoring the change in the MRE value at 222 nm as a function of temperature. Samples were at protein concentrations of 3 μM in 10 mM MOPS, pH 7.0, containing chloride salts of the indicated cations (total ionic strength of 1 M); grey, MOPS alone (total ionic strength 4 mM); K^+, blue; Na^+, black; Li^+, green; Mg^{2+}, orange; Ca^{2+}, maroon; (*C*) fold changes in K_d values compared to condition with no salt. The values were obtained from fitting chemical denaturation data. The ionic strength corresponding to each condition is indicated next to the ion.

Table 1. Parameters from fitting the two-state dimerization model to the data for IF_1-Y33W-H49K at various pH values

pH	ΔG, kcal mol^{-1} [a]	K_d, nM[a]
6 (n=1)	10.15	36.13
7 (n=3)	10.84±0.09	11.30±1.82
8 (n=2)	10.93±0.09	9.72±1.51

[a] Errors denote standard deviations

Table 2. Parameters obtained by fitting the three-state tetramerization model to the data of IF_1-Y33W at various pH values

pH	ΔG_1, kcal mol^{-1} [a]	ΔG_2, kcal mol^{-1} [a]	K_{d1}, nM [a]	K_{d2}, nM [a]
6 (n=1)	8.30	9.42	811.25	122.33
7 (n=3)	11.75±0.07	10.15±0.09	2.42±0.26	36.16±5.76
8 (n=1)	12.70	10.43	0.48	22.47

ΔG_1 and K_{d1} refer to the tetramer/dimer transition; ΔG_2 and K_{d2} refer to the dimer/monomer transition; [a] errors denote standard deviations.

***SI Appendix* for:**

Extrinsic Conditions Influence the Self-Association and Structure of IF_1, the Regulatory Protein of Mitochondrial ATP Synthase

Vytaute Boreikaite[a,b], Basile I. M. Wicky[b], Ian N. Watt[a], Jane Clarke[b] and John E. Walker[a]

[a]*The Medical Research Council Mitochondrial Biology Unit, University of Cambridge, Cambridge Biomedical Campus, Hills Road, Cambridge CB2 0XY, United Kingdom;* [b]*The Department of Chemistry, University of Cambridge, Lensfield Road, Cambridge CB2 1EW, United Kingdom*

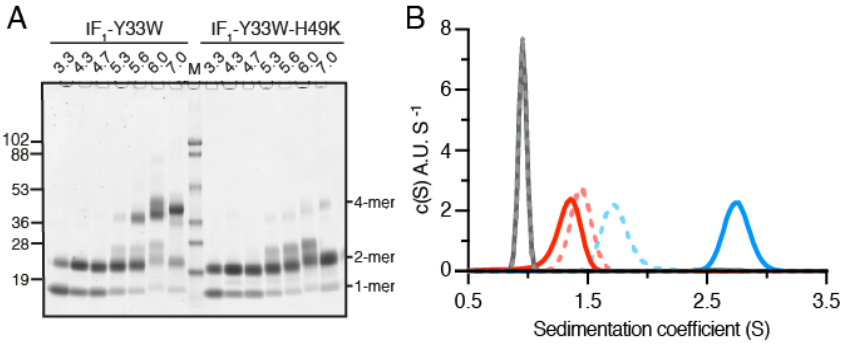

Fig. S1. Dependence of the oligomerization of IF_1 on pH. (*A*) analysis by SDS-PAGE of IF_1-Y33W and IF_1-Y33W-H49K cross-linked with EDC. The pH of each reaction is indicated above the corresponding lane. M, molecular weight marker, with the positions of individual marker proteins indicated on the left; (*B*) sedimentation distribution derived from sedimentation velocity experiments as a function of pH values of 2.4 (grey), 4.0 (red) and 6.9 (blue). Solid lines, IF_1-Y33W; dashed lines, IF_1-Y33W-H49K. See *SI Appendix*, Table S1 for a summary of the data.

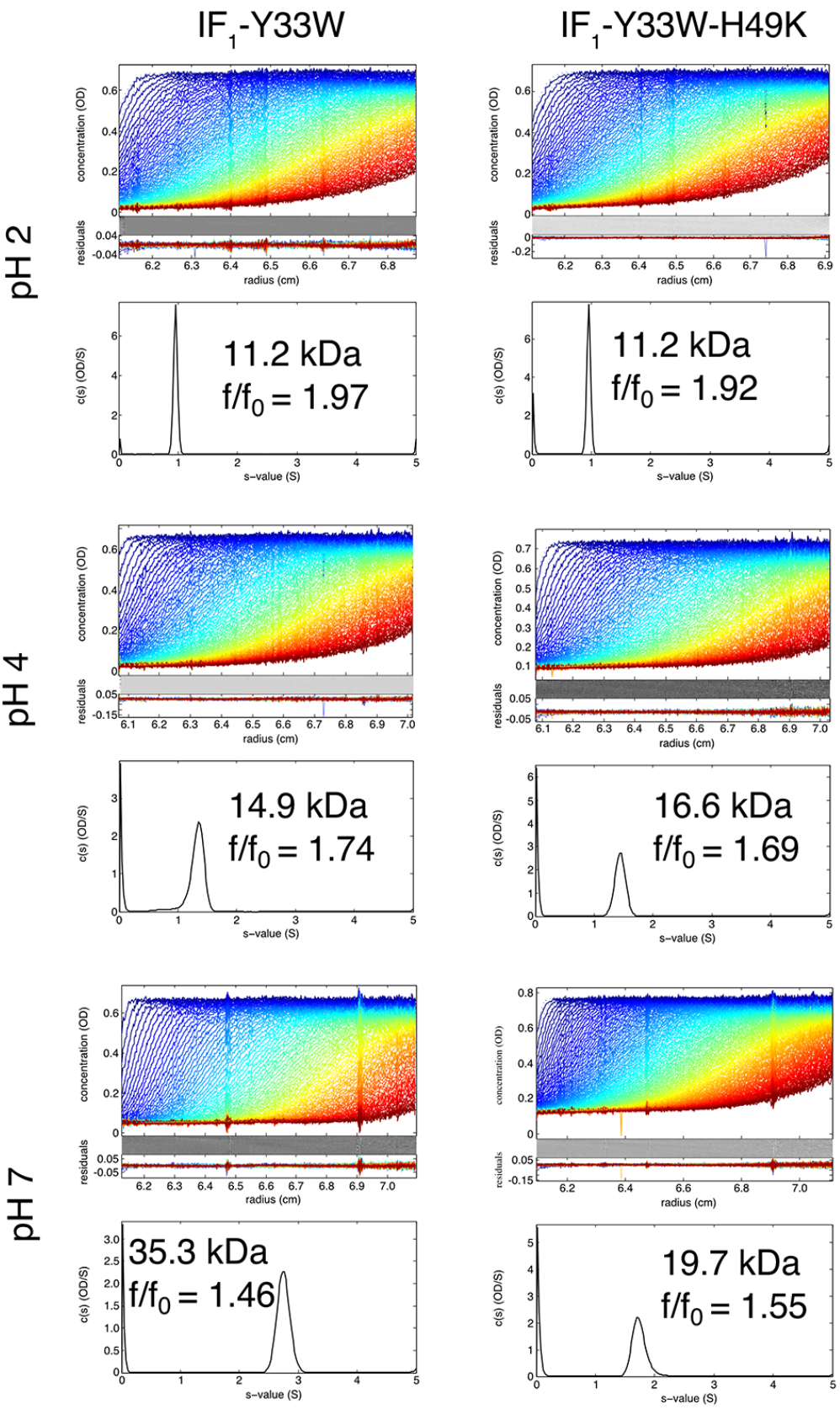

Fig. S2. Sedimentation velocity data. For each protein and each pH value, the

sedimentation boundary as a function of time is indicated (blue to red). Residuals to the fits are indicated below the data, and the sedimentation distribution plots are beneath.

Table S1. Fitted parameters from AUC experiments

	IF_1-Y33W				IF_1-Y33W-H49K			
pH	Mass, kDa	f/f_0	S	$S_{20,w}$	Mass, kDa	f/f_0	S	$S_{20,w}$
2.4	11.2	1.97	0.96	0.96	11.2	1.92	0.96	0.96
4.0	14.9	1.74	1.31	1.31	16.6	1.69	1.44	1.45
6.9	35.3	1.46	2.75	2.79	19.7	1.55	1.75	1.77

The calculated molecular masses of the monomeric proteins are: IF_1-Y33W, 9,604.5 Da; IF_1-Y33W-H49K, 9,595.6 Da; f/f_0, fractional ratio; S, sedimentation coefficient; $S_{20,w}$, corrected sedimentation coefficient (water at 20°C).

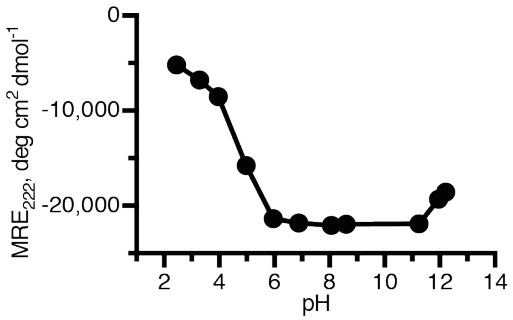

Fig. S3. Influence of pH on the α-helical content of IF_1-Y33W from pH 2.0-12.5. The protein concentration was 6 μM.

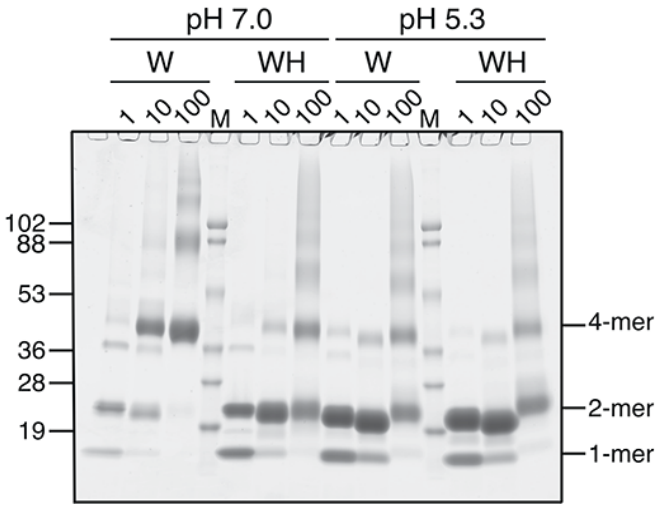

Fig. S4. Influence of protein concentration and pH on the distribution of oligomeric states. Analysis by SDS-PAGE of IF_1-Y33W (W) and IF_1-Y33W-H49K (WH) cross-linked with EDC at pH 5.3 or 7.0 at protein concentrations of 1 µM, 10 µM or 100 µM as indicated above each lane. M, molecular weight marker, with the positions of individual markers indicated on the left.

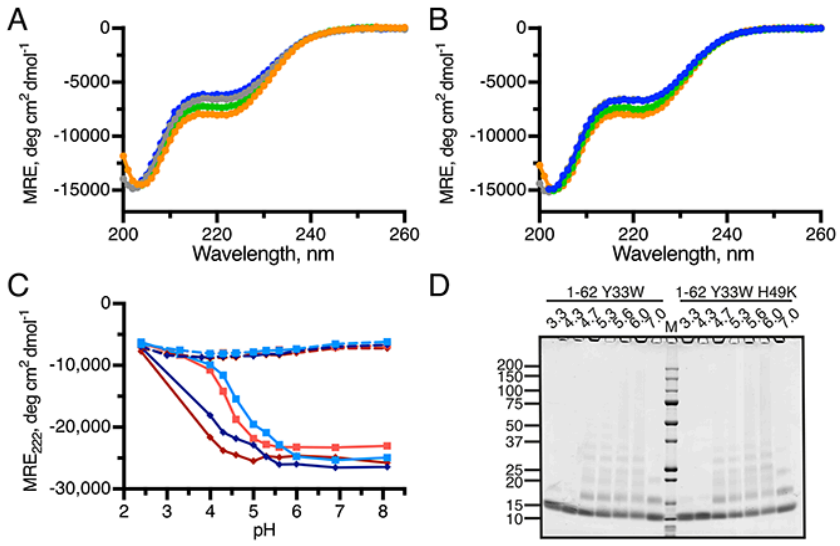

Fig. S5. Effect of pH on the secondary structures and oligomeric states of C-terminally truncated versions of IF_1. (*A*)-(*B*), CD spectra of I1-62-Y33W and I1-62-Y33W-H49K, respectively, at protein concentrations of 100 µM at pH values of 2.4 (red), 4.0 (orange), 6.0 (green) and 8.1 (blue); (*C*) comparison among the profiles of pH dependence of IF_1-Y33W, IF_1-Y33W-H49K, I1-62-Y33W and I1-62-Y33W-H49K at protein

concentrations of 10 μM and 100 μM. IF_1 1-84 Y33W: 10 μM; 100 μM. IF_1-Y33W-H49K: 10 μM; 100 μM. I1-62-Y33W: 10 μM; 100 μM. I1-62-Y33W-H49K: 10 μM; 100 μM; (*D*) SDS-PAGE analysis of I1-62-Y33W and I1-62-Y33W-H49K at protein concentrations of 10 μM cross-linked with EDC at the pH values indicated above each lane. M, molecular weight marker, with the positions of marker proteins indicated on the left.

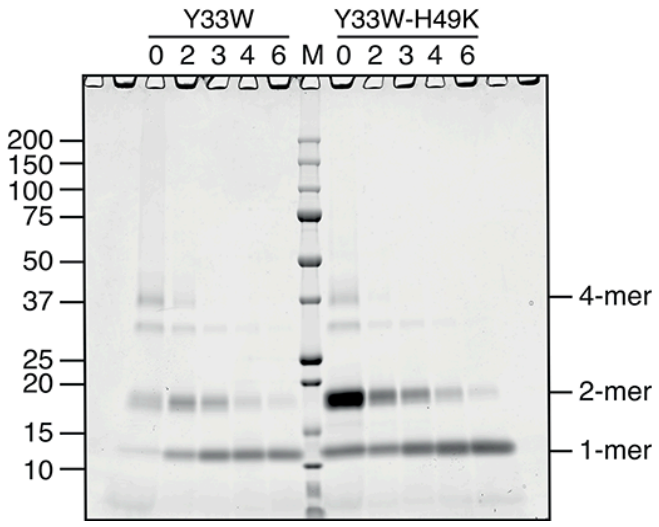

Fig. S6. Analysis by SDS-PAGE of urea-denatured cross-linked proteins. The molarities of urea are indicated above each lane. M, molecular weight marker, with the positions of marker proteins indicated on the left.

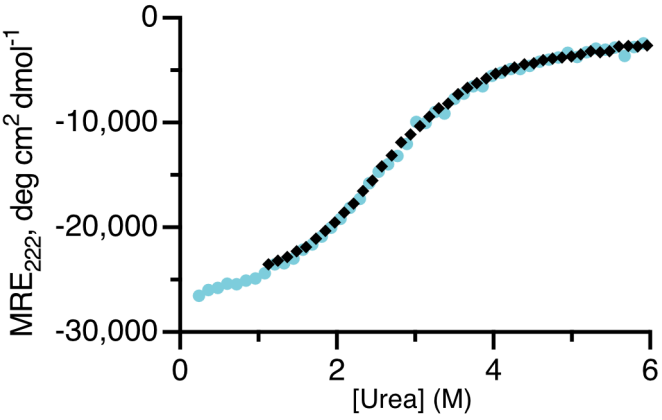

Fig. S7. Reversibility of chemical denaturation experiments. Chemical denaturation data for IF_1-Y33W-H49K at pH 7.0. Unfolding data are denoted by blue dots, and refolding data by black dots.

Table S2. Parameters obtained by fitting the homo-dimerization model to the data of IF_1-Y33W-H49K at pH 7.0

μM	Δ*G*, kcal mol^{-1}	K_d, M	*m*, kcal $mol^{-1}M^{-1}$	S_D	a_D	S_M	a_M
1	10.88	1.04×10^{-8}	1.09	-22,463.7	187.54	-6209.68	730.57
1	10.73	1.34×10^{-8}	1.02	-22,108.4	254.27	-4191.49	395.92
10	10.90	1.01×10^{-8}	1.09	-22,642.2	797.52	-4,731.02	480.23

S_D, dimer base-line, deg cm^2 $dmol^{-1}$; a_D, slope of dimer base-line, deg cm^2 $dmol^{-1}M^{-1}$; S_M, monomer base-line, deg cm^2 $dmol^{-1}$; a_M, slope of monomer base-line, deg cm^2 $dmol^{-1}M^{-1}$.

Table S3. Solvent accessible area and m-values for oligomerization of IF_1

Oligomeric state or transition	ΔSASA, $Å^2$	ΔSASA, $Å^2$	m^c, kcal mol^{-1} M^{-1}	m^d, kcal mol^{-1} M^{-1}	m^e, kcal mol^{-1} M^{-1}
tetramer[a]	20,056	-	-	-	-
dimer[a]	10,952	-	-	-	-
unfolded monomer[b]	10,106	-	-	-	-
dimer-monomer	-	9,261	1.39	1.30	1.08
tetramer-monomer	-	20,368	2.61	2.85	3.45

[a] Calculated with PyMol from the tetramer structure (PDB:1GMJ). The dimer value corresponds to the average solvent accessible area (SASA) from the two dimers present in the structure. [b] Calculated with the web-server ProtSA (33, 34). [c] Calculated from the relationship between ΔSASA and *m*-values reported in (35). [d] Calculated from the

relationship between ΔSASA and *m*-values reported in (24). [e] Average from all experimentally determined values of IF_1-Y33W-H49K (dimer-monomer) or IF_1-Y33W (tetramer-monomer, m_1+2m_2).

Table S4. Parameters obtained by fitting the 2-state tetramerization model to data of IF_1-Y33W at pH 7.0

μM	Δ*G*, kcal mol^{-1}	K_d, M	*m*, kcal mol^{-1}M^{-1}	S_T	a_T	S_M	a_M
1	27.10	1.33×10^{-20}	1.39	-31,151.1	-3,957.51	-8,852.89	1,064.71
3	26.29	5.20×10^{-20}	1.49	-27,194.2	-3,175.45	-6,763.38	732.14
9	25.17	3.45×10^{-19}	1.50	-26,441.1	-2,461.4	-7,095.74	777.33

S_T, tetramer base-line, deg cm^2 dmol^{-1}; a_T, slope of tetramer base-line, deg cm^2 dmol^{-1}M^{-1}; S_M, monomer base-line, deg cm^2 dmol^{-1}; a_M, slope of monomer base-line, deg cm^2 dmol^{-1}M^{-1}.

Table S5. Complete set of parameters from fitting the three-state tetramerization model to data for IF_1-Y33W at pH 7.0

μM	ΔG_1, kcal mol^{-1}	ΔG_2, kcal mol^{-1}	K_{d1}, M	K_{d2}, M	m_1, kcal mol^{-1} M^{-1}	m_2, kcal mol^{-1} M^{-1}	S_T	S_M	a_M
1	11.82	10.16	2.13×10^{-9}	3.55×10^{-8}	1.25	0.85	-27,338.9	-3,771.69	213.48
3	11.72	10.24	2.51×10^{-9}	3.08×10^{-8}	1.27	1.00	-25,020.2	-5,315.92	534.17
9	11.70	10.05	2.63×10^{-9}	4.22×10^{-8}	1.35	0.98	-25,035.0	-4,699.24	456.14

S_T, tetramer baseline, deg cm^2 dmol^{-1}; S_M, monomer baseline, deg cm^2 dmol^{-1}; a_M, slope of monomer baseline, deg cm^2 dmol^{-1} M^{-1}.

Table S6. Masses of purified bovine inhibitor proteins determined by electro-spray ionization mass spectrometry.

Protein	Calculated (Da)	Measured (Da)	Difference (Da)
IF_1-Y33W	9604.5	9604.2	-0.3
IF_1-Y33W-H49K	9595.6	9595.6	-0.4
IF_1-1-62-Y33W	6926.5	6926.2	-0.3
IF_1-1-62-Y33W-H49K	6917.6	6917.1	-0.5

Supplementary Methods

Construction of Expression Plasmids. Residues 1-84 of mature bovine IF_1 correspond to residues 26-109 of the pro-protein in the UniProt entry P01096. The mutation Y33W was introduced by site directed mutagenesis into expression plasmids for mature bovine IF_1 and IF_1-H49K cloned into the vector pRun (36). The following primers were employed in the introduction of the mutation and amplification the plasmid:

IF_1-Y33W For: AGGAGCGATGGTTCCGAGCTCGTGCTAAAGAACAGCTGGCC

IF_1-Y33W Rev: GCTCGGAACCATCGCTCCTCTTCGGCCTGCTCTCTTTTTCC

Template DNA was eliminated by digestion with *DpnI* and the mutated plasmids were transformed into *E. coli* XL1. The DNA sequences were confirmed (Source Biosciences). The final encoded protein sequences were as follows:

IF_1-Y33W: GSESGDNVRSSAGAVRDAGGAFGKREQAEEER**W**FRARAKEQLA-ALKKH**H**ENEISHHAKEIERLQKEIERHKQSIKKLKQSEDDD

IF_1-Y33W-H49K: GSESGDNVRSSAGAVRDAGGAFGKREQAEEER**W**FRARAK-E QLAALKKH**K**ENEISHHAKEIERLQKEIERHKQSIKKLKQSEDDD.

Each of the protein sequences of IF_1-Y33W and IF_1-Y33W-H49K was truncated by the introduction of a stop codon immediately following the codon for residue 62. In addition, a 5'-coding sequence for a hexahistidine tag was introduced before codon 1 with an intervening site for cleavage of the protein with the cysteine protease from tobacco etch virus (TEV). These changes were achieved with two rounds of PCR with each of the two versions of the expression plasmid pRun, one encoding IF_1-Y33W, and the other IF_1-Y33W-H49K. The primers for the first round of PCR were:

IF_1-1-62-For1: 5'AAAACTTGTATTTCCAGGGCTCGGAATCGGGAGATAATG3'

IF_1-1-62-Rev: 5'AATTAAGCTTTAACGTTCAATCTCCTTTGCATGATGAG3'

In the second round of PCR, the product of the first round of PCR was employed as template with the following primers:

IF_1-1-62-For2: 5'AATTCATATGAGCCACCACCACCACCACCACTCTGCGGAA-AACTTGTATTTCCAGGGC 3'

IF_1-1-62Rev (see above).

The resulting PCR products were cloned into pRun and the DNA sequences of the plasmids were verified (Source Biosciences).

The final encoded protein sequences were as follows:

IF_1-1-62-Y33W: MSHHHHHHSAENLYFQGSESGDNVRSSAGAVRDAGGAFGK-REQAEEER**W**FRARAKEQLAALKKHHENEISHHAKEIER

IF_1-1-62-Y33W-H49K: MSHHHHHHSAENLYFQGSESGDNVRSSAGAVRDAGG-AFGKREQAEEER**W**FRARAKEQLAALKKH**K**ENEISHHAKEIER

Protein Expression and Purification. IF_1-1-84-Y33W and IF_1-1-84-Y33W-H49K were expressed in *E. coli* C41 as described before (4). Cells were broken with a Constant Systems cell disrupter and the broken cells were centrifuged (234,000g; 45 min). The supernatant was heated at 70°C for 15 min and then centrifuged (6787g, 15

min). IF_1 was purified from the resulting supernatant by a combination of cation and anion exchange chromatography (4). Fractions containing pure IF_1 were pooled, and the identities of proteins were confirmed by mass spectrometry. IF_1-1-62-Y33W and IF_1-1-62-Y33W-H49K were expressed in the same manner as the full-length inhibitor proteins. Bacterial pellets were resuspended in buffer A (20 mM Tris-HCl, pH 7.4, 0.1 M NaCl and 10 mM imidazole) plus one Complete EDTA free protease inhibitor tablet (Roche), and broken with a constant cell disruptor. The broken cells were centrifuged (234,000g; 45 min; 4°C). The supernatants were loaded onto HisTrap columns (5 ml; GE Healthcare) and IF_1-1-62-Y33W and IF_1-1-62-Y33W-H49K were eluted with a gradient of imidazole from 10-500 mM. Fractions containing IF_1-1-62-Y33W and IF_1-1-62-Y33W-H49K were pooled and dialyzed for 16 h against buffer A (2 l) containing 1 mM (tris(2-carboxyethyl)-phosphine in the presence of the TEV protease. The cleaved histidine tag was removed by passing the dialyzed material through a HisTrap column (1 ml). The integrity of the cleaved products was confirmed by mass spectrometry. All proteins were exchanged from buffer solutions into ultra-pure water by passage through a PD-10 desalting column (GE Healthcare), lyophilized and stored in powder form at 4°C.

Protein Concentrations. For each experiment, fresh samples of IF_1 and truncated and mutated forms were reconstituted by dissolving protein powders in ultra-pure water, containing TWEEN® 20, unless indicated otherwise. The final concentration of TWEEN® 20 in the resuspension solution was 0.05% v/v (see below). The concentrations of these protein stocks were determined from their absorbance at 280 nm measured in a Cary 60 UV-Vis Spectrophotometer (Agilent). Absorbances readings were converted to concentrations with an empirical extinction coefficient (λ_{280}=5,619.4 M^{-1} cm^{-1}). The extinction coefficient was established from a solution of known

concentration as determined by amino acid analysis. As all of the samples of IF_1 and mutant forms contain the same number of aromatic residues, the same value of extinction coefficient was used for all of them. The stocks of IF_1 in water were diluted by weight in appropriate buffers (see below) to achieve the required concentrations of protein for biophysical experiments.

Buffers. Buffers for pH studies were prepared as 10× stocks and used at 1× dilutions (10 mM of buffering component and 8 mM ionic strength, corrected with NaCl if necessary). Buffers for salt studies were prepared as 2× stocks and used at 1× dilutions (10 mM MOPS pH 7.0 and various ionic strength values as indicated in the text). All buffer stocks were prepared volumetrically with sodium salts as conjugate bases and chloride salts as conjugate acids. The buffers for the pH experiments were made at 10× concentration. The buffers contained the following buffering components at a final concentration of 10 mM at 1× dilution: phosphate for pH values of 2.4, pH 3.0, pH 3.3; acetate for pH 3.8, pH 4.0, pH 4.3, pH 4.6; MES for pH 5.0, pH 5.3, pH 5.6, pH 6.0; MOPS for pH 6.9; Tris for pH 8.1. Whenever possible, in the pH experiments, the total ionic strength of the buffers used at 1× dilution was 8 mM. If necessary, the ionic strength was adjusted with NaCl. The buffers used for the salt experiments were prepared at 2× concentration, and contained MOPS as a buffering agent (10 mM at 1× dilution). The ionic strength of these buffers varied as indicated, and was adjusted with appropriate chloride salts. Urea solutions for equilibrium chemical denaturation experiments were prepared gravimetrically and volumetrically with the same buffer stocks, and stored at -20°C to suppress isomerization of urea to ammonium cyanate. Denaturant concentrations were verified from the refractive indices of the solutions compared to buffer (at 25°C), and using the following equation (37):

$$[\text{Urea}] = 117.66(\Delta h) + 29.753(\Delta h)^2 + 185.56(\Delta h)^3$$

where Δh is the difference of refractive index between denaturant and buffer solutions at the sodium D-lines.

Covalent Cross-Linking. Variants of IF_1 in various buffer conditions were covalently cross-linked for 8 h at room temperature in the presence of a 500-fold molar excess of EDC (ThermoFisher) over monomer. When possible, buffers were kept identical to those used in CD experiments. However, because EDC reacts with carboxyl groups and primary amines, the cross-linking buffers for pH 7.0 and pH 4.3 were prepared with phosphate, and at pH 4.7 with MES. Investigations of the dependence of cross-linking on pH were carried out in the absence of TWEEN® 20 to avoid the effect of the detergent on the migration of proteins in analytical SDS-PAGE gels, and the reactions were quenched by addition of loading dye. Samples were heated at 75°C for 10 min, and analyzed on 10-20% Tris-glycine gels (ThermoFisher). Proteins were stained with InstantBlue™ (Expedeon). Investigations of the effects of protein concentration and urea on cross-linking were performed in the presence of TWEEN® 20, to reduce protein loss due to surface adsorption in low concentration samples. The samples at a concentration of 1 μM were concentrated and then analyzed by SDS-PAGE. To prevent anomalous migration patterns due to concentrated salt and detergent contents, the reactions were first quenched with 1% v/v acetic acid-NaOH, pH 4.5, buffer-exchanged into ultra-pure water on a PD-10 desalting column, and stirred overnight with BioBeads SM-2 (Bio-Rad) to remove TWEEN® 20. The proteins were lyophilized and analyzed by SDS-PAGE.

Analytical Ultracentrifugation. IF_1-Y33W and IF_1-Y33W-H49K were dissolved in ultra-pure water without TWEEN® 20, to avoid changes in the density and viscosity of the solutions, and interference with the optics of the instrument. The protein samples were diluted with an appropriate 10× buffer (prepared as described above) to give a

final concentration of protein of 100 μM in 1× buffer at pH 2.4, 4.0 or 6.9. The analytical ultra-centrifugation experiments were carried out in a Beckman Optima XL-I analytical ultracentrifuge. The protein samples and the matched buffer samples were centrifuged for ~20 h at 182,000 g at 20°C. Proteins were detected from their absorbance at 278 nm. Partial specific volumes of the proteins and the densities and the viscosities of the buffers were calculated with SEDNTERP (38). The fitting was done with SEDFIT using a continuous distribution model (39).

CD Spectroscopy. CD experiments were performed with a Chirascan circular dichroism spectrometer (Applied Photophysics) thermostated at 25°C, unless stated otherwise. The contributions of buffers were subtracted from the signals and the signals from proteins were converted to mean residual ellipticity (MRE) units with the following relationship:

$$(\mathrm{MRE}/\,\mathrm{deg}\cdot\mathrm{cm}^2\cdot\mathrm{dmol}^{-1}) = \frac{(\theta/\mathrm{mdeg})}{(l/\mathrm{mm})\ \cdot\ (c/\mathrm{M})\ \cdot\ n}$$

where θ represents the signal from the protein in mdeg, l is the optical path length (in mm), c the concentration (in M), and n the number of amino acids in the protein. MRE values allow direct comparisons between different conditions of protein length and concentration to be made.

Structural scans were recorded from 200-260 nm at 1 nm intervals for 2-10 s per data point (depending on the magnitude of the signal) with adaptive sampling and a bandwidth of 2 nm. In melting experiments, the temperature was raised in steps, and scans (1 nm data intervals, 2 s adaptive sampling, 2 nm bandwidth) were acquired every 2(±0.2) degrees. Data were acquired from 10-90°C. In chemical denaturation experiments, only the dichroic signal at 222 nm was recorded (time-averaging; 30 s per data point, 2 nm bandwidth), and this value was used a proxy for the overall helicity.

Helical contents were estimated from MRE values at 222 nm by the method of Muñoz and Serrano (40), which consists of a linear interpolation between parameters representing a pure α-helix, and a pure coil:

$$\%\ \text{Helicity} = 100 \cdot \left(1 + \frac{(\text{MRE}_{222} - \text{MRE}_{\text{helix}})}{(\text{MRE}_{\text{coil}} - \text{MRE}_{222})}\right)^{-1}$$

where $\text{MRE}_{\text{helix}}$ is the value of a 'pure' α-helical structure at 25°C (-35,791 deg cm^2 dmol^{-1}), and MRE_{coil} represents the value of a 'pure' coil at the same temperature (-725 deg cm^2 dmol^{-1}).

Equilibrium Chemical Denaturation. Equilibrium denaturation curves were determined from 68 samples of increasing concentration of urea, ranging from 0 to 8 M. Buffer/denaturant solutions (800 µL total volume) were dispensed with a Microlab 500 liquid handling unit (Hamilton), and then protein solution (100 µl) was added in the same buffer. Samples were kept at 25°C for 1-3 h and then measurements were made. Changes in MRE_{222} as a function of urea concentration were fitted to appropriate models to extract thermodynamic parameters (see below). Fitting was performed by non-linear least squares minimization routines from Wolfram Mathematica (Wolfram Research), and values of the parameters used during initialization were varied to assess the robustness of the fit and to confirm the convergence of the model.

Quantifying Homo-Oligomerization by Chemical Denaturation. The premise of chemical denaturation studies is based on the observation that the free energy of proteins (folding and/or binding) varies linearly with the concentration of denaturant (37, 41):

$$\Delta G_{[\text{den}]} = \Delta G_{\text{buffer}} - m \cdot [\text{den}]$$

where $\Delta G_{[den]}$ represent the stability of the system at a given concentration of denaturant, ΔG_{buffer} is the stability in buffer, and m is a proportionality constant which relates to the change in solvent accessible surface area (ΔSASA) upon unfolding (35). In the context of multimerization events, knowledge of the binding free energy ($\Delta G_{binding}$) is useful as it relates directly to the equilibrium dissociation constant (K_d) of the reaction:

$$K_d = \exp\left(\frac{\Delta G_{binding}}{RT}\right)$$

where R is the ideal gas constant, and T represents the thermodynamic temperature. Therefore, it is possible to estimate the affinity of an oligomer by analyzing equilibrium chemical denaturation data of its assembled state(s).

Homo-dimerization. If a homo-dimer exists either as a complex or in the monomeric state (*i.e.* 2-state, no intermediate), the dissociation reaction can be described by the following scheme:

$$D \Leftrightarrow 2\,M$$

The equilibrium dissociation constant is expressed by:

$$K_d = \frac{[M]^2}{[D]}$$

The total protein concentration (expressed in terms of monomer) is described by $[M]_T = [M] + 2[D]$, and the equilibrium constant can be expressed as a function of the total concentration of protein and the concentration of dimer:

$$K_d = \frac{([M]_T - 2[D])^2}{[D]}$$

This expression corresponds to a quadratic equation with two solutions. The one with physical meaning is:

$$[D] = \frac{(4[M]_T + K_\mathrm{d}) - \sqrt{(4[M]_T + K_\mathrm{d})^2 - 16[M]_T{}^2}}{8}$$

The fraction of dimer f_D can be expressed by:

$$f_D = \frac{2[D]}{[M]_T}$$

and $f_D + f_M = 1$, where f_M is the fraction of monomer. In an ensemble spectroscopic technique (*e.g.* CD), the observed signal (S) is described by:

$$S = f_M \cdot S_M + f_D \cdot S_D$$

$$= S_M + (S_D - S_M) \cdot f_D$$

where S_M and S_D correspond to the spectroscopic signals of the monomer and dimer respectively. By combining these equations, the observed spectroscopic signal can be expressed by:

$$S = S_M + (S_D - S_M) \cdot \frac{(4[M]_T + K_\mathrm{d}) - \sqrt{(4[M]_T + K_\mathrm{d})^2 - 16[M]_T{}^2}}{4\,[M]_T}$$

and for a chemical denaturation experiment, the equilibrium dissociation constant is substituted by:

$$K_\mathrm{d} = \exp\left(-\frac{(\Delta G_\mathrm{buffer} - m[\mathrm{den}])}{RT}\right)$$

which results in the following expression:

$$S = S_M + (S_D - S_M) \cdot \frac{\left(4[M]_T + \exp\left(-\frac{(\Delta G_\mathrm{buffer} - m[\mathrm{den}])}{RT}\right)\right) - \sqrt{\left(4[M]_T + \exp\left(-\frac{(\Delta G_\mathrm{buffer} - m[\mathrm{den}])}{RT}\right)\right)^2 - 16[M]_T{}^2}}{4\,[M]_T}$$

where [den] is the independent variable, S is the dependent variable, S_M, S_D, m, and ΔG_buffer are fitting parameters, and $[M]_T$ is a known quantity. This equation was used to fit chemical denaturation data for IF_1-Y33W-H49K. Under certain conditions, the spectroscopic signals of the species are not independent of the denaturant concentration (*i.e.* 'sloping baselines'). In such cases, linear correction terms can be applied:

$$S_x = S_x^{\text{buffer}} + a_x \cdot [\text{den}]$$

where S_x is the observed spectroscopic signal of species *x* at a given concentration of denaturant, S_x^{buffer} its signal in buffer, and a_x a constant of proportionality. These expressions were substituted for the terms S_M and S_D.

Homo-tetramerization (2-state). The framework for studying homo-tetramerization reactions is fundamentally identical, but requires the solutions to polynomial functions of degree four.

Starting with the case of a 2-state (no intermediate) homo-tetramerization reaction (*i.e.* only the tetrameric and monomeric states are populated at equilibrium), the reaction scheme can be expressed by:

$$T \Leftrightarrow 4\,M$$

The equilibrium dissociation constant of the reaction is described by:

$$K_{\text{d}} = \frac{[M]^4}{[T]}$$

which can be re-written as:

$$K_{\text{d}} = \frac{([M]_T - 4[T])^4}{[T]}$$

This equation is a quartic with four analytical solutions, one of which is physically meaningful. By analogy to the framework described for homo-dimerization reactions, the spectroscopic signal for a 2-state homo-tetramerization reaction can be expressed as:

$$S = S_M + (S_T - S_M) \cdot \frac{4\,[T]}{[M]_T}$$

where $[T]$ represent the solution of the quartic equation (expressed in terms of $[A]_T$ and K_{d}, which is itself expressed in terms of free energy as described for the homo-dimerization case). Thus, *S* (the dependent variable) can be expressed as a function of

[den] (the independent variable), with four fitting parameters (S_M, S_T, m, and ΔG_{buffer}), and one known quantity ($[M]_T$). If necessary, linear terms can be added to the spectroscopic signal of each species to account for denaturant dependencies.

Homo-tetramerization (3-state). The dissociation of a homo-tetramer *via* a dimeric intermediate can be expressed by the following scheme:

$$T \Leftrightarrow 2\,D \Leftrightarrow 4\,M$$

The dissociation constant corresponding to each equilibrium are expressed as:

$$K_1 = \frac{[D]^2}{[T]} \quad \text{and} \quad K_2 = \frac{[M]^2}{[D]}$$

Here the second equilibrium is expressed for the dissociation of *one* dimer. Thus, the overall equilibrium constant is:

$$K = K_1 K_2 K_2$$

As for the previous cases, the observed spectroscopic signal can be expressed as a linear combination of spectroscopic signal associated with each species, multiplied by their fractional contribution to the ensemble:

$$S = f_T \cdot S_T + f_D \cdot S_D + f_M \cdot S_M$$

Using the definitions for the equilibrium constants, and the relationship describing the total concentration of monomer ($[M]_T = 4[T] + 2[D] + [M]$), the fraction of each species can be expressed in terms of the concentration of monomer, the *total* concentration of monomer, and the individual dissociation constants (*N.B.* the choice of [*M*] is arbitrary, and analogous expressions could be obtained in terms of [*D*] or [*T*]):

$$f_T = \frac{4[M]^4}{[M]_T K_1 K_2 K_2}$$

$$f_D = \frac{2[M]^2}{[M]_T K_2}$$

$$f_M = \frac{[M]}{[M]_T}$$

In these expressions, [*M*] is the unknown. By using the definition of the equilibrium constants and the total concentration of monomer, the following relationship can be expressed:

$$0 = K_2\,[M]_T - K_2[M] - 2[M]^2 - \frac{4[M]^4}{K_1K_2}$$

This equation is a quartic with respect to [*M*], and possesses four analytical solutions; one of which is physically meaningful (Supplementary Equation 2). Thus, the observed spectroscopic signal (*S*) can be expressed as a function of the dissociation constants (K_1 and K_2), the total concentration of monomer ($[M]_T$), and the spectroscopic signal corresponding to each species (S_T, S_D, S_M).

Finally, for chemical denaturation experiments, the equilibrium constants are expressed in terms of free energy as:

$$K_1 = \exp\left(-\frac{\left(\Delta G_1^{\text{buffer}} - m_1[\text{den}]\right)}{RT}\right)$$

$$K_2 = \exp\left(-\frac{\left(\Delta G_2^{\text{buffer}} - m_2[\text{den}]\right)}{RT}\right)$$

where $\Delta G_1^{\text{buffer}}$ and $\Delta G_2^{\text{buffer}}$ are the free energy of dissociation (in buffer) for the tetramer and dimer respectively, and m_1 and m_2 are their respective constants of proportionality (which correspond to the ΔSASA associated with each dissociation). Note that $\Delta G_2^{\text{buffer}}$is defined per mole of dimer, thus $\Delta G_{\text{tot}}^{\text{buffer}} = \Delta G_1^{\text{buffer}} + 2\,\Delta G_2^{\text{buffer}}$.

Therefore, for a 3-state homo-tetramerization reaction, the observed spectroscopic signal (*S*, the dependent variable) can be expressed as a function of [den] (the independent variable), seven fitting parameters ($\Delta G_1^{\text{buffer}}$, $\Delta G_2^{\text{buffer}}$, m_1, m_2, S_T, S_D, S_M), and the known quantity $[M]_T$. As described previously, linear correction terms can be added to spectroscopic signal of each species if necessary.

Fitting the Data of Chemical Denaturation Experiments. The homo-dimerization

model described above was used to fit the equilibrium chemical denaturation data of IF_1-Y33W-H49K. The values of free energy obtained from three independent datasets at pH 7.0 matched closely, demonstrating the robustness of this fitting strategy (*SI Appendix*, Table S2). Also, the *m*-values did not vary significantly with changes in protein concentration. This confirms the absence of an intermediate, validating the use of the 2-state homo-dimerization model to fit the data of IF_1-Y33W-H49K (24). The average *m*-value (~1.1 kcal mol^{-1} M^{-1}) is also consistent with the expected □SASA for dimerization, further validating the use of this model (*SI Appendix*, Table S3).

Due to the absence of a clear intermediate in the unfolding transition of IF_1 Y33W, the data were fitted first to the 2-state homo-tetramerization model. However, all parameters showed a trend with increasing protein concentration (*SI Appendix*, Table S4). This behavior suggested that the wrong model had been employed. In addition, the fitted slopes for the tetramers were negative, suggesting that the tetramer becomes more folded with increasing denaturant concentration, which is unlikely (*SI Appendix*, Table S4). Moreover, the *m*-value obtained from fitting the 2-state model (~1.5 kcal mol^{-1} M^{-1}) is significantly smaller than expected from ΔSASA calculations (*SI Appendix*, Table S3). Finally, a change in *m*-value has been shown to indicate the presence of an intermediate (24, 42, 43). Taken together, these shortcomings indicated that the 2-state homo-tetramerization model did not properly describe the experiments, and suggested that an intermediate was present on the energy landscape. Therefore, the data were fitted to the 3-state homo-tetramerization model, which captured the data accurately (*vide infra*).

When sloping baselines are included for each species, the 3-state model comprises ten parameters. This led to convergence problems during fitting routines, and the compensation of certain parameters by others, indicating a lack of robustness of the

fit. Therefore, an alternative to free fitting was found, and some simplifying assumptions were made. The thermodynamic parameters (ΔG_1, ΔG_2, m_1, m_2) and the baselines corresponding to the tetramer and the monomer were left unconstrained. Sloping baselines for the tetramer and the dimer were not included in order to reduce the number of parameters, and since these states are mostly folded, they were not expected to be very sensitive to changes in denaturant concentration. However, the slope for the monomer was kept, as this state is unfolded, and, therefore, it is likely to be affected by changes in denaturant concentrations. Finally, the baseline for the dimeric intermediate was fixed to the value of IF_1-Y33W-H49K (-23,000 deg cm^2 $dmol^{-1}$); a valid assumption given that these two states are structurally related. It is noted that the numerical choice of this value did not affect the other fitted parameters significantly. With this strategy, the number of free fitting parameters was reduced to seven, and fitting routines became robust (Table S5). This approach was used to fit all the chemical denaturation data for IF_1-Y33W (pH and salt). We note that the *m*-value obtained for the tetramer/dimer transition is slightly larger than the *m*-value associated with the dimer/monomer transition. Given that the latter involves both folding and binding, this result might at first appear surprising. However, since the dimer is expected to be a simple coiled-coil (limited buried core), and that tetramerization represents a dimerization of dimers (more residues involved per event), the relative and absolute magnitude of these numbers appear reasonable.

Equation S1. Solution to the quartic equation relative to the 2-state hetero-tetramerization reaction. P represent the total monomer concentration ($[M]_T$).

$$
\begin{aligned}
T &= \frac{1}{16}\left(4P \right. \\
&- \frac{\sqrt{\left(54\mathrm{Kd}^2 - 6\sqrt{3}\sqrt{\mathrm{Kd}^3(27\mathrm{Kd} + 1024P^3)}\right)^{1/3} - \frac{86^{2/3}\mathrm{Kd}P}{\left(9\mathrm{Kd}^2 - \sqrt{3}\sqrt{\mathrm{Kd}^3(27\mathrm{Kd} + 1024P^3)}\right)^{1/3}}}}{\sqrt{3}} \\
&- 8\sqrt{\left(\frac{\mathrm{Kd}P}{4\left(54\mathrm{Kd}^2 - 6\sqrt{3}\sqrt{\mathrm{Kd}^3(27\mathrm{Kd} + 1024P^3)}\right)^{1/3}}\right.} \\
&- \frac{\left(9\mathrm{Kd}^2 - \sqrt{3}\sqrt{\mathrm{Kd}^3(27\mathrm{Kd} + 1024P^3)}\right)^{1/3}}{326^{2/3}} \\
&\left. - \frac{\sqrt{3}\mathrm{Kd}}{16\sqrt{\left(54\mathrm{Kd}^2 - 6\sqrt{3}\sqrt{\mathrm{Kd}^3(27\mathrm{Kd} + 1024P^3)}\right)^{1/3} - \frac{86^{2/3}\mathrm{Kd}P}{\left(9\mathrm{Kd}^2 - \sqrt{3}\sqrt{\mathrm{Kd}^3(27\mathrm{Kd} + 1024P^3)}\right)^{1/3}}}}\right)\Bigg)
\end{aligned}
$$

Equation S2. Solution to the quartic equation relative to the 3-state hetero-tetramerization reaction. P represent the total monomer concentration ($[M]_T$).

$$
\begin{aligned}
M = \tfrac{1}{4\sqrt{6}}\Big(&\sqrt{(-8\mathrm{K1K2}+2}: \\
&(8\mathrm{K1}^3\mathrm{K2}^3+18\mathrm{K1}^2\mathrm{K2}^3(3\mathrm{K2}+16P)-6\sqrt{3}\sqrt{\mathrm{K1}^3\mathrm{K2}^6(1024P^3+8\mathrm{K1}^2(\mathrm{K2}+8P)+\mathrm{K1}(27\mathrm{K2}^2+288\mathrm{K2}P+512P^2))})^{1/3} \\
&+(42^{2/3}\mathrm{K1K2}^2(\mathrm{K1}-12P))/(4\mathrm{K1}^3\mathrm{K2}^3+9\mathrm{K1}^2\mathrm{K2}^3(3\mathrm{K2}+16P)-3\sqrt{3}\sqrt{\mathrm{K1}^3\mathrm{K2}^6(1024P^3+8\mathrm{K1}^2(\mathrm{K2}+8P)+\mathrm{K1}(27\mathrm{K2}^2+288\mathrm{K2}P+512P^2))})^{1/3})\Big) \\
&-\frac{1}{2}\sqrt{\left(-\frac{2\mathrm{K1K2}}{3}-(\mathrm{K1K2}^2(\mathrm{K1}-12P))/(3(8\mathrm{K1}^3\mathrm{K2}^3+18\mathrm{K1}^2\mathrm{K2}^3(3\mathrm{K2}+16P)-6\sqrt{3}\sqrt{\mathrm{K1}^3\mathrm{K2}^6(1024P^3+8\mathrm{K1}^2(\mathrm{K2}+8P)+\mathrm{K1}(27\mathrm{K2}^2+288\mathrm{K2}P+512P^2))})^{1/3}\right)} \\
&-\frac{1}{62^{2/3}}(4\mathrm{K1}^3\mathrm{K2}^3+9\mathrm{K1}^2\mathrm{K2}^3(3\mathrm{K2}+16P)-3\sqrt{3}\sqrt{\mathrm{K1}^3\mathrm{K2}^6(1024P^3+8\mathrm{K1}^2(\mathrm{K2}+8P)+\mathrm{K1}(27\mathrm{K2}^2+288\mathrm{K2}P+512P^2))})^{1/3} \\
&-(\sqrt{6}\mathrm{K1K2}^2)\Big/\Big(\sqrt{(-8\mathrm{K1K2}+2\left(8\mathrm{K1}^3\mathrm{K2}^3+18\mathrm{K1}^2\mathrm{K2}^3(3\mathrm{K2}+16P)-6\sqrt{3}\sqrt{\mathrm{K1}^3\mathrm{K2}^6\left(1024P^3+8\mathrm{K1}^2(\mathrm{K2}+8P)+\mathrm{K1}(27\mathrm{K2}^2+288\mathrm{K2}P+512P^2)\right)}\right)^{1/3}} \\
&+(42^{2/3}\mathrm{K1K2}^2(\mathrm{K1}-12P))/(4\mathrm{K1}^3\mathrm{K2}^3+9\mathrm{K1}^2\mathrm{K2}^3(3\mathrm{K2}+16P)-3\sqrt{3}\sqrt{\mathrm{K1}^3\mathrm{K2}^6(1024P^3+8\mathrm{K1}^2(\mathrm{K2}+8P)+\mathrm{K1}(27\mathrm{K2}^2+288\mathrm{K2}P+512P^2))})^{1/3})\Big)
\end{aligned}
$$